

Temporal Variation of Close-Proximity Soundings within a Tornadoic Supercell Environment

Kentaro Araki, Hiroshi Ishimoto, Masataka Murakami, and Takuya Tajiri
Meteorological Research Institute, Tsukuba, Japan

Abstract

We examined proximity soundings at intervals of a few minutes and at distances of less than 20 km from a significant tornadoic (SIGTOR) supercell that occurred on 6 May 2012 in Japan. We used a 1-dimensional variational (1DVAR) technique that combined the observations of a ground-based microwave radiometer with outputs from a numerical model. Based on the results of the 1DVAR, several supercell and tornado forecast parameters were calculated and compared with values typical of SIGTOR supercell environments in the United States. One and a half hours before the occurrence of the tornado, the value of convective available potential energy increased significantly to about 1000 J kg^{-1} , a value that is smaller than the typical value in the United States. Low-level vertical wind shear and some composite parameters attained maximum values at the time when the distance to the supercell was the smallest. The vertical wind shear parameters and some composite parameters indicated that the environment fell into the SIGTOR supercell category. This result shows that the thermodynamic environments became unstable before the approach of the supercell, and the low-level vertical wind shear changed locally near the supercell.

(Citation: Araki, K., H. Ishimoto, M. Murakami, and T. Tajiri, 2014: Temporal variation of close-proximity soundings within a tornadoic supercell environment. *SOLA*, **10**, 57–61, doi:10.2151/sola.2014-012.)

1. Introduction

Both observations and numerical simulations have been used to examine the dynamic and thermodynamic environments of significant tornadoic (SIGTOR) supercells, but the prediction and nowcast of SIGTOR supercells remain challenging because of a lack of understanding of the environments favorable for supercells. To understand the environments of tornadoic supercells and to identify criteria that can help forecasters estimate the timing, location, and intensity of supercells, previous studies have used model analyses (e.g., Thompson et al. 2003; hereafter T03) and proximity soundings made with radiosondes within supercell environments (e.g., Rasmussen and Blanchard 1998; Potvin et al. 2010). T03 examined thermodynamic, vertical wind shear, and composite parameters derived from proximity soundings that were obtained from the Rapid Update Cycle-2 analysis and forecast system within supercell environments in the United States. T03 divided the soundings into three types: nontornadoic, weakly tornadoic (F0-F1 tornado damage), and SIGTOR (F2-F5 tornado damage) supercells. They found that vertical wind shear and moisture within 1 km of the surface can discriminate between nontornadoic and SIGTOR supercells. Although T03 investigated spatial and temporal proximity soundings with resolutions of 40 km and 1 hour, no study of proximity soundings within SIGTOR supercell environments has provided information on temporal variations at intervals of a few minutes. For nowcasting purposes, understanding of temporal variations of tornadoic supercell environments is required on a timeframe of minutes.

Recently, ground-based microwave radiometer profilers

(MWR) and neural network (NN) techniques (MWR_NN; Solheim et al. 1998) have been used to obtain vertical thermodynamic profiles of air temperature and water vapor density at time intervals of a few minutes (e.g., Ware et al. 2003, 2013). The capabilities of the MWR_NN-derived profiles have been investigated (e.g., Cimini et al. 2006), and some studies have applied the profiles to the analysis of convective storms (e.g., Knupp et al. 2009; Madhulatha et al. 2013; Ratnam et al. 2013). In addition, some recent studies have shown that 1-dimensional variational (1DVAR) techniques that combine radiometric observations with outputs from a numerical weather model outperform other temperature and water vapor profiling retrieval methods (e.g., Hewison et al. 2007; Cimini et al. 2010, 2011; Ishimoto 2014).

The purpose of this study was to use proximity and high-frequency soundings to examine the details of the temporal variation of a SIGTOR supercell environment in Japan. One of the strongest tornadoes (rank F3) since 1960 in Japan occurred in the northern part of the Tsukuba city, on the Kanto Plain, on 6 May 2012. MWR observations were successfully conducted at the Meteorological Research Institute (MRI) in Tsukuba at distances less than 20 km from the tornado. We used a 1DVAR technique to obtain the thermodynamic profiles and examined the temporal variations of several supercell and tornado forecast parameters by using both 1DVAR-derived thermodynamic profiles and wind profiles from the results of a numerical simulation.

2. Data and methods

We used the ground-based MWR (MP-3000A, Radiometrics) installed at the MRI in Tateno (in Tsukuba), at 36.05°N , 140.13°E . The MWR observes the brightness temperatures of 21 K-band (22–30 GHz) and 14 V-band (51–59 GHz) microwave channels at multiple elevation angles, the radiation temperature of one zenith-looking infrared (9.6–11.5 μm wavelength) channel, and the in situ surface temperature, relative humidity, and pressure. In this study, we used the data from the zenith-looking microwave channels. The vertical profiles of air temperature and water vapor density up to a height of 10 km and precipitable water vapor (PWV) and liquid water path (LWP) were retrieved by using a NN technique (Solheim et al. 1998), which uses statistical inversion techniques to combine MWR observations with radiosonde climatology. Vertical retrieval intervals were 50 m from the surface to 500 m, 100 m to 2 km, and 250 m to 10 km. The NN was trained by using a series of historical radiosonde data from the Japan Meteorological Agency (JMA) station at Tateno. Figure 1 shows the comparisons of MWR_NN-derived variables and daily radiosonde profiles between 25 April and 27 June 2012 (129 soundings) when no rain was observed within 1 hour before or after radiosonde observations (89 soundings). The radiosonde measurements were interpolated according to the MWR altitude resolution, and MWR_NN-derived variables were averaged for 30 minutes after the radiosonde observations. These temperature profiles showed good agreement; the absolute mean difference (MD) was less than 1 K below 3.5 km (Fig. 1a). The standard deviation (STD) and root mean square error (RMSE) for the MWR_NN-derived temperatures were less than 2 K below 4.5 km and 3.5 km, respectively. The MD of water vapor density was negative below 3 km, and the absolute MD was less than 1.4 g m^{-3} below 500 m, $0.5\text{--}1 \text{ g m}^{-3}$ between 500 m and 1 km, and $0\text{--}0.5 \text{ g m}^{-3}$ between 1 km and 3 km (Fig. 1b). Similar results have been reported by Cimini et al. (2006). The PWVs were derived from the NN as

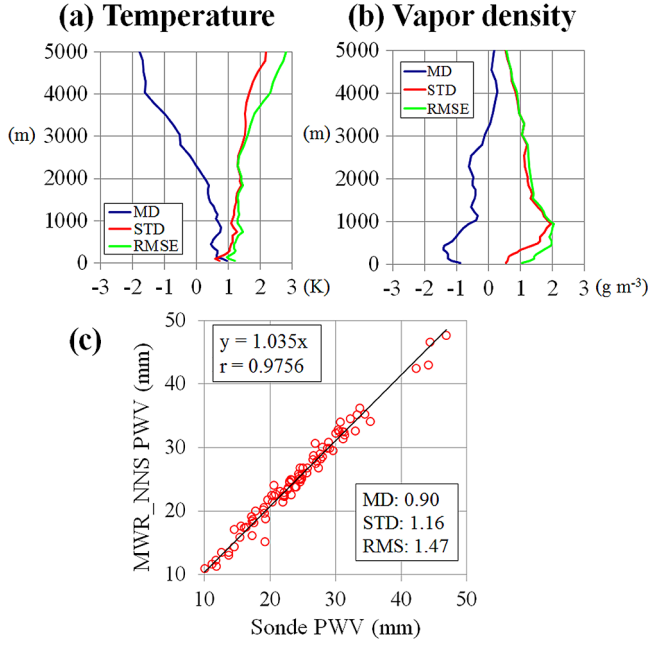


Fig. 1. Mean difference (MD), standard deviation (STD) and root-mean-square error (RMSE) of MWR_NN-derived (a) air temperature and (b) water vapor density with respect to radiosonde soundings (89 cases). (c) Comparison of MWR_NNS-derived and radiosonde-derived PWVs. The black solid line $y = 1.035x$ is a regression line.

scalar values (MWR_NNS) and were in very good agreement with sonde-derived PWVs, the correlation coefficient and MD being 0.9756 and 0.9 mm, respectively (Fig. 1c).

The details of the 1DVAR technique used in this study are given by Ishimoto (2014). In this method, retrieval variables \mathbf{x} are composed of profiles of air temperature and water vapor density, and liquid water path. The iterative solution that minimizes the cost function is given by

$$\mathbf{x}_{i+1} = \mathbf{x}_i + (\mathbf{B}^{-1} + \mathbf{H}_i^T \mathbf{R}^{-1} \mathbf{H}_i)^{-1} [\mathbf{H}_i^T \mathbf{R}^{-1} (\mathbf{y} - \mathbf{F}(\mathbf{x}_i)) - \mathbf{B}^{-1} (\mathbf{x}_i - \mathbf{x}_b)]$$

where \mathbf{x}_i and \mathbf{x}_b are current and background state vectors, respectively; \mathbf{H}_i is the Jacobian matrix of the observation vector with respect to the state vector; \mathbf{B} and \mathbf{R} are the error-covariance matrices of \mathbf{x}_i and of the observation vector \mathbf{y} , respectively; and $\mathbf{F}(\mathbf{x}_i)$ is the forward model operator.

The numerical model used in this study was the JMA Non Hydrostatic Model (NHM; Saito et al. 2006). We performed an experiment with a horizontal grid spacing of 1 km and a model domain covering the Kanto Plain. The initial and boundary conditions were provided from 3-hourly JMA mesoscale analyses. The integration time was from 0600 to 2200 Japan standard time (JST; JST = UTC + 9 h) on 6 May 2012. The time step of the NHM was 6 seconds, and the results were output at 5-minute intervals. A convection parameterization scheme was not used. Other setups were the same as those used by Saito et al. (2006). Profiles averaged in $5 \text{ km} \times 5 \text{ km}$ squares centered at Tateno were interpolated to MWR observation times and used for the 1DVAR.

Supercell and tornado forecast parameters were calculated from the soundings derived from the MWR_NN, NHM, and 1DVAR and were compared with the analogous parameters of the SIGTOR supercell environments reported in T03. We used the same method as T03 to calculate the mean layer (0–1 km) convective available potential energy (MLCAPE) and lifted condensation level (MLLCL) as thermodynamic parameters. Vertical wind shear parameters of the storm relative helicity of 0–1 and 0–3 km (SRH1km, SRH3km) were calculated using storm motions estimated by the algorithm of Bunkers et al. (2000). Since wind profiler data at Tateno, which was collected not for operational purpose but for research purpose, was available only in the lower

layer, vertical wind shear parameters were calculated by using the NHM-derived wind profiles. T03 has shown that the SRH1km's based on both Bunkers algorithm and observed supercell motion have similar values. The SRH1km and SRH3km were therefore compared with those of T03 based on observed supercell motions. We also calculated the magnitude of the wind shear vector from the surface to an altitude of 6 km (SHR6km). As composite parameters, we calculated the mean layer energy-helicity index (MLEHI), the mean layer bulk Richardson number (MLBRN), the supercell composite parameter (SCP), and the significant tornado parameter (STP). The MLEHI identifies tornado potential as follows:

$$\text{MLEHI} = (\text{MLCAPE} \times \text{SRH1km}) / 160,000.$$

The MLBRN is proportional to the MLCAPE and inversely proportional to the vertical wind shear through the lowest 6 km:

$$\text{MLBRN} = \text{MLCAPE} / 0.5(U^2)$$

where U represents the difference between the density-weighted mean winds in the 0–6 km and 0–500 m layers. SCP identifies the environments of supercells and nonsupercells, and STP identifies the environments of SIGTOR and nontornadic supercells. SCP is given by

$$\text{SCP} = (\text{MUCAPE} / 1000 \text{ J kg}^{-1}) \times (\text{SRH3km} / 100 \text{ m}^2 \text{ s}^{-2}) \times (\text{BRN shear} / 40 \text{ m}^2 \text{ s}^{-2})$$

where MUCAPE is the convective available potential energy based on the most unstable parcel in the lowest 3 km, and the bulk Richardson number (BRN) shear is the denominator of the MLBRN. STP is given by

$$\text{STP} = (\text{MLCAPE} / 1000 \text{ J kg}^{-1}) \times (\text{SHR6km} / 20 \text{ m s}^{-1}) \times (\text{SRH1km} / 100 \text{ m}^2 \text{ s}^{-2}) \times [(2000 - \text{MLLCL}) / 1500 \text{ m}].$$

3. Results

The Tsukuba F3 tornado occurred 13–17 km northwest of Tateno from 1235 to 1251 JST on 6 May 2012 (Fig. 2a). Yamauchi et al. (2013) used C-band polarimetric radar to investigate the structure of the tornado and noted that the parent storm of the tornado was a classic supercell. Figure 2a shows the surface air temperature and wind at 1300 JST observed by the Automated Meteorological Data Acquisition System (AMeDAS) of the JMA and by the Atmospheric Environmental Regional Observation System of the Japanese Ministry of the Environment. Figure 2a also shows the Plan Position Indicator (PPI) reflectivity observed by JMA Tokyo Doppler radar at an elevation angle of 1.7° at 1252 JST. A supercell with a well-defined hook echo moved east-northeastward along the low-level convergence line formed by warm southwesterly and cold northwesterly flows to the northwest of Tateno. The distance from Tateno to the hook echo decreased from 50 km to less than 20 km from 1200 to 1240 JST. The AMeDAS observed warm southerly flows and no rainfall at Tateno during the event. These conditions were suitable for the MWR at Tateno to observe the supercell environment. The results of the NHM at 1245 JST are shown in Fig. 2b. The environmental fields and a supercell with a well-defined hook echo, consistent with observations, were successfully reproduced. Temporal variation of simulated wind profiles were also compared with the observed profiles at three stations in the Kanto plain, and were consistent to the observations during the event (not shown). However, the simulated movement of the supercell was about 5 minutes ahead of the observed movement.

Time-height cross sections of air temperature and water vapor density derived from the MWR_NN, NHM, 1DVAR, and the difference between the 1DVAR and the NHM between 0900 and 1500 JST are shown in Figs. 3 and 4. The MWR_NN-derived temperature profiles showed the warmest layer below 500 m (Fig. 3a), although the warm layer thickness was larger in the NHM-derived profiles than in the MWR_NN-derived profiles. The 1DVAR-derived temperatures below 2 km were lower by 0.5–2 K and

were intermediate between the NHM-derived and MWR_NN-derived soundings (Fig. 3d). In terms of water vapor density, a low-level layer with high water vapor density (over 12 g m^{-3}) was apparent below 300 m in the MWR_NN-derived profiles (Fig. 4a). A thin layer with very high water vapor density (over 14 g m^{-3}) was also apparent near the ground, and the water vapor density between 500 m and 1 km ranged from 7 to 10 g m^{-3} in the same profiles. In contrast, in the NHM-derived profiles, the thickness of the layer with water vapor density greater than 12 g m^{-3} was about 1 km. Even considering the tendency of the MWR_NN-derived water vapor density between altitudes of 500 m and 1 km to be underestimated by $0.5\text{--}1 \text{ g m}^{-3}$, the NHM-derived water vapor

density between 500 m and 1 km still seems too high. The 1DVAR-derived profiles also successfully reduced the high water vapor density between 500 m and 1 km by more than 1.5 g m^{-3} , and the 1DVAR-derived profiles were intermediate between the NHM-derived and MWR_NN-derived water vapor density profiles (Fig. 4d). According to Ishimoto (2014), the NHM often overestimated air temperature in the boundary layer below 1 km, and the 1DVAR technique successfully improved the profile of air temperature and water vapor density below 1 km compared with radiosonde observations during a field campaign in Kochi in June 2010. A similar superiority of 1DVAR-derived profiles over NHM-derived profiles is also apparent in this study.

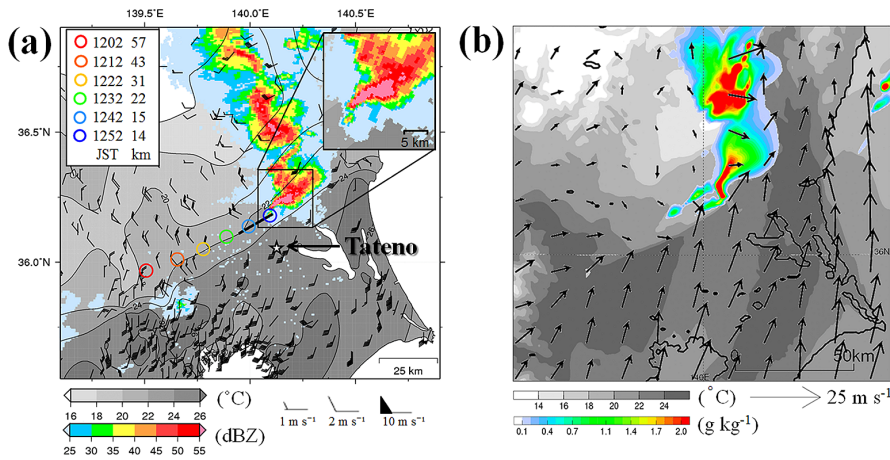


Fig. 2. Observed and NHM-simulated environments of the tornadic supercell on 6 May 2012. (a) Surface air temperature (gray), wind (barbs) at 1300 JST, and PPI reflectivity observed by Tokyo Doppler radar at an elevation angle of 1.7° at 1252 JST. (b) Horizontal distribution of simulated quantities at 1245 JST; air temperature (gray) and wind (vectors) at a height of 20 m above the surface and mixing ratios of hydrometers (color shading; sum of rainwater, snow, and graupel) at a height of 1 km above sea level. The white star and the black solid line in (a) indicate the location of Tateno and the path of the tornado, respectively. Colored circles indicate the locations of the hook echo observed on the PPIs at the same elevation angle; the observation times and the distances from Tateno are shown in the upper-left corner of (a).

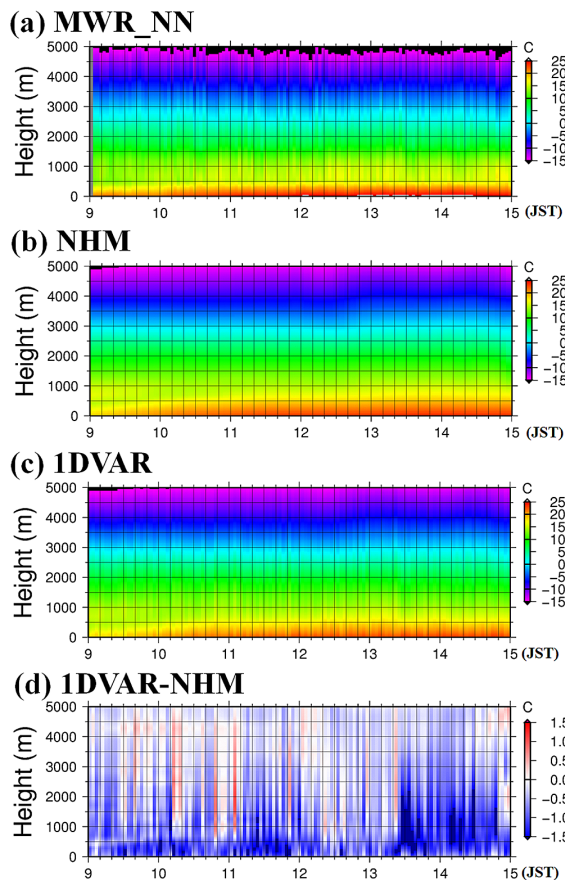


Fig. 3. Time-height cross sections of (a) MWR_NN-derived, (b) NHM-derived, (c) 1DVAR-derived air temperatures, and (d) the difference between 1DVAR-derived and NHM-derived air temperatures.

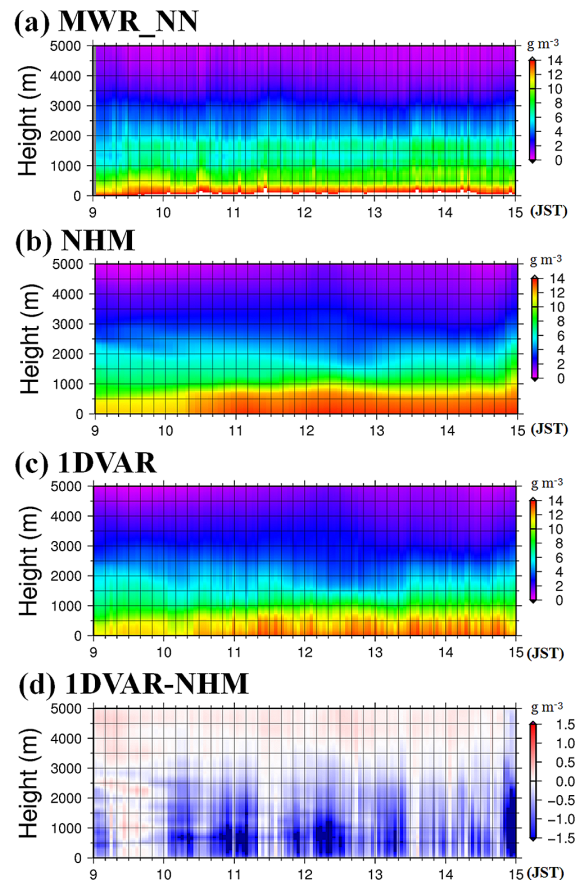


Fig. 4. Same as Fig. 3, but for water vapor density.

To assess the water vapor error during the event, we compared the PWVs obtained from the integration of water vapor profiles derived by the MWR_NN, NHM, and 1DVAR with the MWR_NNS-derived PWV (Fig. 5). Because the MWR_NNS-derived PWV proved to be accurate (Fig. 1c), we conclude that the MWR_NN (NHM)-derived PWVs were underestimated (overestimated). In contrast, the 1DVAR-derived PWVs showed good agreement with the MWR_NNS-derived PWVs. This result suggests that the 1DVAR technique successfully reproduced the probable water

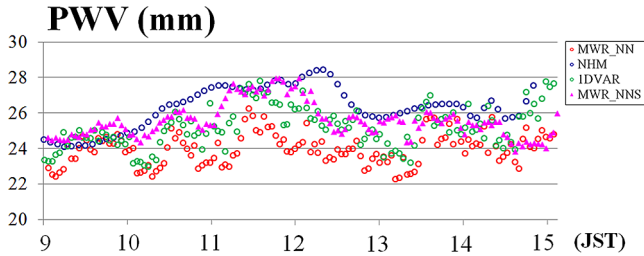


Fig. 5. Time series of PWVs obtained from the integration of water vapor profiles derived from the MWR_NN algorithm, NHM simulation, and 1DVAR technique, and the MWR-derived scalar values (MWR_NNS) of PWV.

vapor profiles during the event.

Time series of thermodynamic, vertical wind shear, and composite parameters between 0900 and 1500 JST are shown in Fig. 6. The numbers in each panel indicate the values of the 10th and 90th percentiles and the median (in parentheses) of each parameter in SIGTOR supercell environments reported by T03. The 1DVAR-derived MLCAPE increased significantly to about 1000 J kg^{-1} 1.5 hours before the occurrence of the tornado, although the value was smaller than the T03 values of 1059–3683 J kg^{-1} (Fig. 6a). MWR_NN-derived and NHM-derived MLCAPE values also increased at the same time, but reached about 750 and 1500 J kg^{-1} , respectively. This difference is due to the thermodynamic states in the 0–1 km layer. A high MLCAPE before the approach of the supercell indicates the existence of environmental conditions favorable for the supercell. The MLLCLs derived from each profile ranged from 1000 to 1300 m during the event and were comparable to typical values. Low MLLCLs in this case were consistent with the suggestion of Markowski et al. (2002) that increased low-level relative humidity contributes to an increase of buoyancy in the rear flank downdraft and occurrence probability of tornadoes.

The vertical wind shear parameters of the SRH1km and SRH3km attained maximum values of 170 and 260 $\text{m}^2 \text{ s}^{-2}$, respectively during the time interval 1230–1250 JST (Fig. 6c). These vertical wind shear parameters are comparable to typical

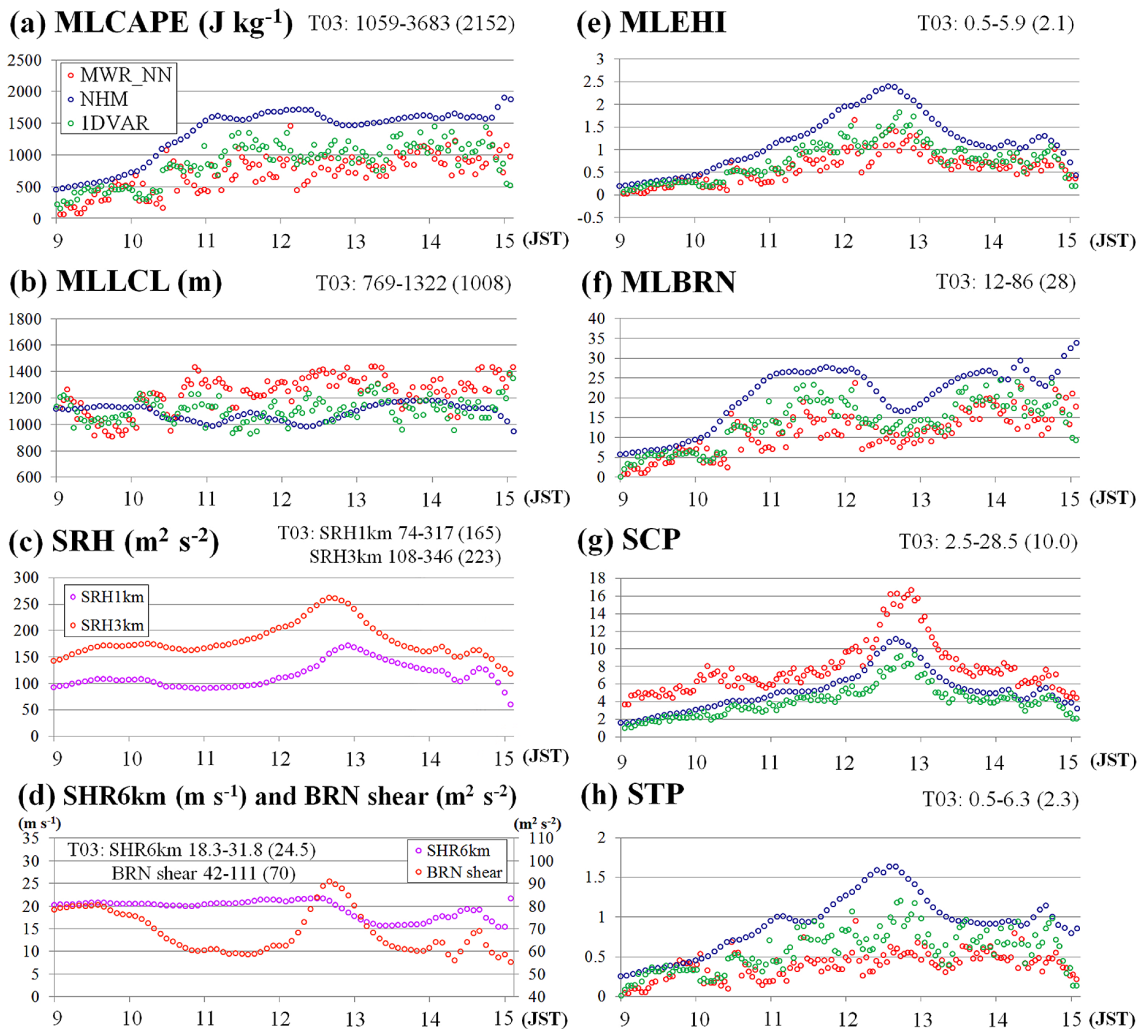


Fig. 6. Time series of parameters derived from MWR_NN-derived, NHM-derived, and 1DVAR-derived soundings: (a) MLCAPE, (b) MLLCL, (e) MLEHI, (f) MLBRN, (g) SCP, and (h) STP. Time series of vertical wind shear parameters derived from NHM-simulated wind profiles: (c) SRH1km and SRH3km, and (d) SHR6km and BRN shear. Numbers in each panel indicate the 10th and 90th percentiles, and the median (in parentheses) of each parameter in the SIGTOR supercell category reported by T03.

values, and indicate that a strong, low-level, vertical wind shear supports the SIGTOR supercell environment. The values of the SHR6km ranged from 20 to 22 m s^{-1} before the end of the tornado at 1250 JST; these values are also comparable to typical values (Fig. 6d). The BRN shear increased from 60 to 90 $\text{m}^2 \text{s}^{-2}$ from 1200 to 1250 JST. Because the typical value of BRN shear is 42–111 $\text{m}^2 \text{s}^{-2}$, the SHR6km and BRN shear during the event indicated that both the 0–1 km and 0–6 km wind shears supported the tornadic supercell environment.

Between 1100 and 1300 JST the 1DVAR-derived MLEHI increased from 0.5 to 1.9, and this range is comparable to typical values (Fig. 6e). The values of the 1DVAR-derived MLBRN between 1100 and 1250 JST were 15–25 (Fig. 6f), which was within the range of typical values, 12–86. The 1DVAR-derived SCP attained a maximum value of about 9 at around 1250 JST, which is also comparable to typical values of 2.5–28.5 (Fig. 6g). The 1DVAR-derived STP also attained a maximum value of 1.2 at around 1250 JST, which was within the range of typical values, 0.5–6.3 (Fig. 6h).

4. Conclusion and remarks

We used the 1DVAR technique to obtain close-proximity, high-frequency, probable soundings within the Tsukuba F3 tornadic supercell environment by combining radiometric observations with the results of a numerical simulation. Although the values of the vertical wind shear parameters in this case were comparable to typical values in the SIGTOR supercell environment in the United States, the value of the 0–1 km MLCAPE was smaller than the typical value.

Sakurai and Kawamura (2008) have examined the thermodynamic and vertical wind shear parameters statistically by using radiosonde soundings within 50 km and two hours of the tornadoes. They showed that the 0–500 m MLCAPE was 66 J kg^{-1} averaged over 47 tornadic events in Japan; this value is much smaller than the typical values of 1059–3683 J kg^{-1} reported in the United States. They noted that the MLCAPE parameter did not help to identify a tornadic environment, although their samples included no classic supercell tornado. Chuda and Niino (2005) investigated climatological monthly statistics of MUCAPE which was calculated by using radiosonde observations, and noted the 90th percentile value of MUCAPE on May at Tateno was 275 J kg^{-1} . This study showed that the MLCAPE increased significantly to about 1000 J kg^{-1} 1.5 hours before the occurrence of the tornado, and although its values were smaller than the typical values in the United States, the MLCAPE could help to identify an environment favorable for a SIGTOR supercell. The low-level vertical wind shear and composite parameters, including the MLEHI, SCP, and STP, attained maximum values at the time when the distance to the supercell was the smallest; these parameter values indicated that the Tsukuba F3 tornadic event occurred under conditions associated with a SIGTOR supercell category. The results of this study also show that thermodynamic environments became unstable before the approach of the supercell and that low-level vertical wind shear changed locally near the supercell.

Although NHM-derived wind profiles were used in this study, wind profiler data would provide vertical wind shear in real time and would be of benefit in terms of operational use. The combination of high-frequency thermodynamic and wind profiles would be of benefit in nowcasting severe storms such as SIGTOR supercells.

Acknowledgements

We would like to express our gratitude to Dr. Y. Shoji of the MRI for his useful advice on the PWV analysis. We are also grateful to the reviewers and the editor. The Japanese Ministry of the Environment and National Institute for Environmental Studies kindly provided surface observations.

References

- Bunkers, M. J., B. A. Klimowski, J. W. Zeitler, R. L. Thompson, and M. L. Weisman, 2000: Predicting supercell motion using a new hodograph technique. *Wea. Forecasting*, **15**, 61–79.
- Chuda, T., and H. Niino, 2005: Climatology of environmental parameters for mesoscale convections in Japan. *J. Meteor. Soc. Japan*, **83**, 391–408.
- Cimini, D., T. Hewison, L. Martin, J. Gueldner, C. Gaffard, and F. Marzano, 2006: Temperature and humidity profile retrievals from ground-based microwave radiometers during TUC. *Meteor. Z.*, **15**, 45–56.
- Cimini, D., E. Westwater, and A. Gasiewski, 2010: Temperature and humidity profiling in the Arctic using ground-based millimeter-wave radiometry and 1DVAR. *IEEE Trans. Geosci. Remote Sens.*, **48**, 4959–4969.
- Cimini, D., E. Campos, R. Ware, S. Albers, G. Giuliani, J. Oreanuno, P. Joe, S. E. Koch, S. Cober, and E. Westwater, 2011: Thermodynamic atmospheric profiling during the 2010 winter Olympics Using ground-based microwave radiometry. *IEEE Trans. Geosci. Remote Sens.*, **49**, 4959–4969.
- Hewison, T., 2007: 1D-VAR retrievals of temperature and humidity profiles from a ground-based microwave radiometer. *IEEE Trans. Geosci. Remote Sens.*, **45**, 2163–2168.
- Ishimoto, H., 2014: Analysis of microwave radiometric data using a 1DVAR technique. *Meteor. Res. Notes*, (in press, in Japanese).
- Knupp, K., T. Coleman, D. Phillips, R. Ware, D. Cimini, F. Vandenberghe, J. Vivekanandan, and E. Westwater, 2009: Ground-based passive microwave profiling during dynamic weather conditions. *J. Atmos. Oceanic Technol.*, **26**, 1057–1073.
- Madhulatha, A., M. Rajeevan, M. Venkat Ratnam, J. Bhate, and C. V. Naidu, 2013: Nowcasting severe convective activity over southeast India using ground-based microwave radiometer observations. *J. Geophys. Res.*, **118**, 1–13.
- Markowski, P. N., J. M. Straka, and E. N. Rasmussen, 2002: Direct surface thermodynamic observations within the rear-flank downdrafts of nontornadic and tornadic supercells. *Mon. Wea. Rev.*, **130**, 1692–1721.
- Potvin, C. K., K. L. Elmore, and S. J. Weiss, 2010: Assessing the impacts of proximity sounding criteria on the climatology of significant tornado environments. *Wea. Forecasting*, **25**, 921–930.
- Rasmussen, E. N., and D. O. Blanchard, 1998: A baseline climatology of sounding-derived supercell and tornado forecast parameters. *Wea. Forecasting*, **13**, 1148–1164.
- Ratnam, M. V., Y. D. Santhi, M. Rajeevan, and S. V. B. Rao, 2013: Diurnal variability of stability indices observed using radiosonde observations over a tropical station: comparison with microwave radiometer measurements. *Atmospheric Research*, **124**, 21–33.
- Saito, K., T. Fujita, Y. Yamada, J. Ishida, Y. Kumagai, K. Aranami, S. Ohmori, R. Nagasawa, S. Kumagai, C. Muroi, T. Kato, H. Eito, and Y. Yamazaki, 2006: The operational JMA nonhydrostatic mesoscale model. *Mon. Wea. Rev.*, **134**, 1266–1298.
- Sakurai, K., and R. Kawamura, 2008: The environment and potential predictability of tornadoes occurred in Japan. *Tenki*, **55**, 7–22 (in Japanese).
- Solheim, F., J. Godwin, E. Westwater, Y. Han, S. Keihm, K. Marsh, and R. Ware, 1998: Radiometric profiling of temperature, water vapor, and cloud liquid water using various inversion methods. *Radio Sci.*, **33**, 393–404.
- Thompson, R. L., R. Edwards, J. A. Hart, K. L. Elmore, and P. Markowski, 2003: Close proximity soundings within supercell environments obtained from the Rapid Update Cycle. *Wea. Forecasting*, **18**, 1243–1261.
- Ware, R., D. Cimini, E. Campos, G. Giuliani, S. Albers, M. Nelson, S. E. Koch, P. Joe, and S. Cober, 2013: Thermodynamic and liquid profiling during the 2010 Winter Olympics. *Atmospheric Research*, **132–133**, 278–290.
- Ware, R., R. Carpenter, J. Gueldner, J. Liljegren, T. Nehr Korn, F. Solheim, and F. Vandenberghe, 2003: A multichannel radiometric profiler of temperature, humidity, and cloud liquid. *Radio Sci.*, **38**, 8079, doi:10.1029/2002RS002856.
- Yamauchi, H., H. Niino, O. Suzuki, Y. Shoji, E. Sato, A. Adachi, and W. Mashiko, 2013: Vertical structure of the Tsukuba F3 tornado on 6 May 2012 as revealed by a polarimetric radar. *Preprints, 36th Conf. on Radar Meteorology, Breckenridge, CO, Amer. Meteor. Soc.*, 320.